Subharmonic and Quasi-Periodic Motions of an Eccentric Squeeze Film Damper-Mounted Rigid Rotor

J. Y. Zhao
Research Officer,
Department of Mechanical Engineering,
Australian Defence Force Academy,
Campbell, ACT 2600,
Australia

I. W. Linnett
Lecturer,
Department of Mechanical Engineering,
Australian Defence Force Academy,
Campbell, ACT 2601,
Australia

L. J. McLean
Associate Director,
Machine Design and Development Manager,
A.E. Bishop & Associates Pty Ltd,
10 Waterloo Road,
North Ryde, NSW 2113, Australia

When a squeeze-film damper is operated eccentrically, the nonlinear damper forces are no longer radially symmetric and subharmonic and quasi-periodic vibrations may be excited by the rotor unbalance. In this study, the unbalance response of a rigid rotor, supported on an eccentric squeeze film damper, is first approximated by a harmonic series whose coefficients are determined by the collocation method, together with a nonlinear least-square regression. The stability of the resulting periodic solution is then examined using the Floquet transition matrix method. For sufficiently large values of the unbalance and the damper static radial misalignment, it is shown that the approximate harmonic motion loses its stability and bifurcates into a stable subharmonic motion and a quasi-periodic motion at speeds above twice the system critical speed. This analytical finding is verified by a numerical integration in forms of the Poincaré map, the rotor trajectory, the bifurcation diagram, and the power spectrum. It is suggested that stability analysis and numerical integration should always be incorporated into an approximate analytical method to achieve an adequate approximation. The results of this study show that the introduction of squeeze-film dampers may give rise to the undesirable nonsynchronous vibrations, which limits the maximum speed at which dampers should be used.

1 Introduction

Squeeze-film damper bearings have been widely used in aero-engines to attenuate resonant vibration and to improve the stability of rotor bearing systems. Since the development of squeeze-film damper bearings, much theoretical attention has been paid to the centered synchronous, circular rotor motion which only exists when the damper is statically centralized. Jump phenomenon of the hardening spring characteristic of cavitated damper models has been reported by many researchers such as White (1970) and Feng (1988). A nonsynchronous mode of operation was mentioned by Mohan and Hahn (1974) and was numerically examined by Li and Taylor (1987).

Botman (1976) observed nonsynchronous vibrations at speeds above twice the system critical speed on a high-speed rigid rotor-damper test rig. Nikolajsent and Holmes (1979) reported their observation of nonsynchronous vibrations in a test rig of a flexible, symmetric rotor on two identical plain journal bearings supported by centralized squeeze-film dampers. The nonsynchronous vibrations occurred at speeds between two and three times the first critical speed. Sykes and Holmes (1990) also reported subharmonic vibrations in a rigid rotor-damper system subjected to an unbalance force and a unidirectional static force.

The difficulty of analyzing the nonsynchronous and noncircular rotor vibration is well known and such analysis may well provide important damper design information. There is no one analytical technique that can accomplish this study effectively. The direct integration of the differential equations has been commonly used but it proves costly in computing time.

The trigonometric collocation method has been used by Nataraj and Nelson (1989) for studying the periodic response of nonlinear dynamic systems. To determine multiple solutions whenever they exist, an arc-length incremental continuation method has been introduced by Zhao, et al. (1992), together with a linear polynomial predictor-corrector algorithm for nonlinear iterations. The Floquet transition matrix method has been extended to investigate the stability of the resulting periodic solutions (Zhao, et al., 1992).

It should be noted that the justification of the trigonometric approximation is solely that it expected that the rotor response will be periodic and can be approximated by a truncated trigonometric series. However, there is no practical criterion to determine which, and how many, frequency components are required to form an adequate approximation. This paper will present an approach for choosing proper frequency components in the trigonometric series. Numerical examples are given for a rigid rotor supported on an eccentric squeeze-film damper. Using the theory of nonlinear dynamics and bifurcations (Arnol'd, 1983), a rigorous analysis of the bifurcation of the approximate solutions will be given. A numerical integration scheme is incorporated to examine the accuracy of the approximation and to find any aperiodic solutions. The numerical integration results are given in forms of the Poincaré map, the

Contributed by the Technical Committee on Vibration and Sound for publication in the JOURNAL OF VIBRATION AND ACOUSTICS. Manuscript received July 1992; revised September 1993. Associate Technical Editor: M. Ahmadian.

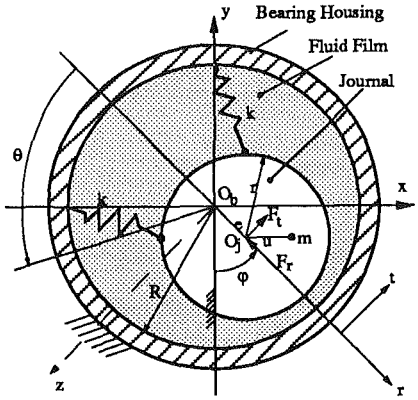

Fig. 1 Cross section of a rigid rotor supported by a squeeze-film damper

bifurcation diagram, the rotor trajectory, and the power spectrum.

2 Approximate Solution

Figure 1 shows a rigid rotor supported on a squeeze-film damper in parallel with retaining springs. To analyze this system, the following assumptions are made:

(*a*) The rotor speed is constant;
(*b*) The rolling element bearings are rigid;
(*c*) The Reynolds equation for constant lubricant properties, the short bearing approximation, and the 'π' film damper model are applicable.

The equations of the rotor motion in Cartesian coordinates can be written as:

$$m\ddot{x}+d\dot{x}+kx=mu\omega^2\cos\omega t+f_x+kx_0, \tag{1}$$

$$m\ddot{y}+d\dot{y}+ky=mu\omega^2\sin\omega t+f_y+ky_0. \tag{2}$$

The origin of the o—xyz-coordinate system is taken to be the bearing center O_b. Dividing these two equations by $mc\omega^2$ and defining a nondimensional time $\tau=\omega t$ and a speed parameter $s=\omega/\omega_n$, one obtains the following nondimensionalized equations of motion:

$$X''+\frac{DX'}{s}+\frac{X}{s^2}=U\cos\tau+\frac{B}{s}\frac{(XF_r-YF_t)}{\epsilon}+\frac{X_0}{s^2}, \tag{3}$$

$$Y''+\frac{DY'}{s}+\frac{Y}{s^2}=U\sin\tau+\frac{B}{s}\frac{(XF_t+YF_r)}{\epsilon}+\frac{Y_0}{s^2}. \tag{4}$$

Using the short bearing approximation and assuming both supply pressure and return pressure to be atmospheric pressure, the pressure distribution in the damper is

$$p=\frac{6\mu\omega L^2\zeta(\zeta-1)(\epsilon'\cos\theta+\varphi'\epsilon\sin\theta)}{c^2(1+\epsilon\cos\theta)^3}. \tag{5}$$

The resulting damper forces in the radial and tangential directions are determined by integrating Eq. (5) over the area of the journal sleeve, viz:

$$(F_r, F_t)=\frac{c^2}{\mu L^2}\int_0^{2\pi}\int_0^1 p(\cos\theta, \sin\theta)d\zeta d\theta. \tag{6}$$

The 'π' film damper model was used by setting p to zero when p was negative. The film forces were evaluated by a two-dimensional numerical integration at each step of the nonlinear iterations. The steady rotor motion was approximated by a trigonometric series of

$$X=a_{x0}+\sum_{i=1}^{N}a_{xi}\cos\mathbf{h}(i)\tau+b_{xi}\sin\mathbf{h}(i)\tau. \tag{7}$$

$$Y=a_{y0}+\sum_{i=1}^{N}a_{yi}\cos\mathbf{h}(i)\tau+b_{yi}\sin\mathbf{h}(i)\tau. \tag{8}$$

The coefficients of the trigonometric series were determined using the collocation method, together with the arc-length continuation algorithm, given by Zhao, et al. (1992).

3 Stability and Bifurcation

It should be noted that, by using the approximate analytical method, one merely finds the equilibrium states, which are only realized when they are stable. To examine the local stability of such an approximate solution $\mathbf{q}_0$, one may investigate the dynamic behavior of the system by superimposing a perturbation $\delta\mathbf{q}$ on $\mathbf{q}_0$, such that

Nomenclature

$a_{x0}, a_{xi}, b_{xi}, a_{y0}, a_{yi}, b_{yi}$ = trigonometric coefficients
$AH(i)$ = semimajor axis of ith frequency component
B = bearing parameter $=\mu RL^2/mc^3\omega_n$
c = damper clearance $=R-r$
D = $d/smc\omega_n^2$
e = damper eccentricity $=\epsilon c$
f_x, f_y, F_r, F_t = damper forces
$\mathbf{h}$ = real vector
L = bearing length
m, d, k = mass, viscous damping, and stiffness
$\mathbf{M}, \mathbf{C}, \mathbf{K}$ = mass, damping and stiffness matrices
N = order of the trigonometric series
O_b, O_j = geometric centers of bearing and damper
p = pressure distribution in damper
$\mathbf{q}$ = displacement vector
r, R = radii of damper and bearing, respectively
r, t = radial and tangent coordinates
s = speed parameter $=\omega/\omega_n$
t = time; $\tau=\omega t$
T = driving period $=2\pi/\omega$
u = mass eccentricity of rotor; $U=u/c$
$\mathbf{u}(i)$ = eigenvalue of transition matrix over one period
x, y, z = horizontal, vertical, and axial coordinates
x_0, y_0 = damper static displacements
X = x/c, $Y=y/c$, $X_0=x_0/c$, $Y_0=y_0/c$
ω = angular speed; $\omega_n=\sqrt{k/m}$ = static resonance
ω_1 = the second fundamental frequency, $\overline{\omega}_1=\omega_1/\omega$
μ = oil dynamic viscosity; $\zeta=z/L$
ϵ_0 = static radial misalignment $=\sqrt{X_0^2+Y_0^2}$
θ = angular position along the lubricant film
φ = angular displacement of line O_bO_j
$(\dot{}), (')$ = derivatives with respect to t and τ

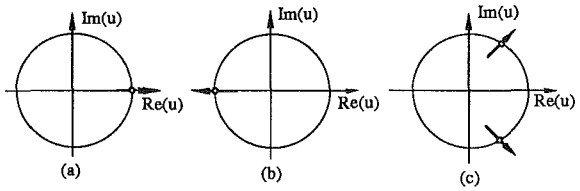

Fig. 2 Three types of losing stability; (*a*) Saddle-node; (*b*) Periodic doubling; (*c*) Torus

$$\mathbf{q} = \mathbf{q}_0 + \delta\mathbf{q}. \tag{9}$$

The perturbed equation of motion is thus

$$\mathbf{M}\delta\ddot{\mathbf{q}} + (\mathbf{C} - \mathbf{Q})\delta\dot{\mathbf{q}} + (\mathbf{K} - \mathbf{P})\delta\mathbf{q} = \mathbf{0}. \tag{10}$$

where

$$\mathbf{q} = \begin{Bmatrix} X \\ Y \end{Bmatrix}, \ \mathbf{M} = \begin{bmatrix} 1 & 0 \\ 0 & 1 \end{bmatrix}, \ \mathbf{C} = \frac{D}{s}\begin{bmatrix} 1 & 0 \\ 0 & 1 \end{bmatrix},$$

$$\mathbf{K} = \frac{1}{s^2}\begin{bmatrix} 1 & 0 \\ 0 & 1 \end{bmatrix}, \ \mathbf{Q} = \begin{bmatrix} \dfrac{\delta F_x}{\delta \dot{X}} & \dfrac{\delta F_x}{\delta \dot{Y}} \\ \dfrac{\delta F_y}{\delta \dot{X}} & \dfrac{\delta F_y}{\delta \dot{Y}} \end{bmatrix}, \ \mathbf{P} = \begin{bmatrix} \dfrac{\delta F_x}{\delta X} & \dfrac{\delta F_x}{\delta Y} \\ \dfrac{\delta F_y}{\delta X} & \dfrac{\delta F_y}{\delta Y} \end{bmatrix}$$

Thus, the stability of $\mathbf{q}_0$ is predicted from the examination of the stability of Eq. (10), which is a set of linear differential equations with $\mathbf{P}$ and $\mathbf{Q}$ being periodic functions of time. Because $\mathbf{P}$ and $\mathbf{Q}$ are periodic, the investigation of the stability of Eq. (10) does not directly reduce to a simple eigenvalue problem.

The Floquet transition matrix method was used by Zhao, et al. (1992) to examine the stability of the system of Eqs. (10). This theory indicates that the knowledge of the state transition matrix over one period is sufficient to determine the stability of the system.

Let $u(i)$, $i = 1, 2, 3, 4$, be the eigenvalues (multipliers) of the transition matrix over one period. According to the Floquet criterion, the necessary and sufficient condition for the periodic solution under investigation to be stable is that the inequalities:

$$|u(i)| = \sqrt{\mathrm{Re}[u(i)]^2 + \mathrm{Im}[u(i)]^2} < 1 \quad \text{for } i = 1, 2, 3, 4$$

are satisfied. If there is no eigenvalue greater than one, but at least one eigenvalue equals one, the stability of $\mathbf{q}_0$ will depend on the nonlinear terms.

The stability of an approximate periodic solution is normally governed by a leading multiplier or a leading pair of complex-conjugate multipliers. The multipliers and, hence, the stability of the predicted unbalance response vary with the rotor speed, s. As the rotor speed is varied, three types of instability, as shown in Fig. 2, may occur depending on the point at which the unit circle is crossed (Arnol'd, 1983). For increasing stability, the arrows in Fig. 2 point at the opposite direction.

In Fig. 2(*a*), the leading multiplier crosses the unit circle is at (1, 0) and the instability of the periodic motion is equivalent to the saddle-node type instability of stationary points and so is referred to as the cycle saddle-node type. Figure 2(*b*) shows the leading multiplier crossing the unit circle at (−1, 0) and the periodic motion becomes unstable and another motion, winding twice per driving cycle, appears—a periodic doubling occurs. In Fig. 2(*c*), the unit circle is crossed at a pair of complex-conjugate multipliers, the periodic motion becomes unstable and bifurcates into a quasi-periodic motion having two irrational fundamental frequencies. This bifurcation is analogous to the Hopf bifurcation of stationary points and, therefore, it is referred to as the secondary Hopf bifurcation.

Whenever the two fundamental frequencies become rational, i.e., the argument angle of the pair of complex-conjugate multipliers equals $\pm m2\pi/n$ (m, n are integers), the quasi-periodic motion will lock into a subharmonic motion of nth order. For example, when the argument angle is $\pm 2\pi/3$, there will be a subharmonic motion of the third order building up from the unstable motion. It can be noted that the periodic doubling bifurcation is a special case with $n = 2$.

4 Numerical Integration

The nondimensional equations of rotor motion were numerically integrated using a fourth-order Runge-Kutta method with a constant time step of $2\pi/120$. To illustrate the numerical results, the following plots are used.

Poincaré Map. A Poincaré section is a stroboscopic picture of a motion in a phase plane and it consists the time series at a constant interval of T ($T = 2\pi/\omega$). The point on the Poincaré section is referred to as the return point. The projection of a Poincaré section on the $X(nT)$-$Y(nT)$-plane is referred as the Poincaré map of the motion, which indicates the nature of motion. In case of a periodic motion, the n discrete points in the Poincaré map indicate that the period of motion is nT. In the case of a two-dimensional torus (quasi-periodic motion), return points appear to fill up a closed curve in the Poincaré map. For a chaotic motion, return points form a geometrically fractal structure.

Bifurcation Diagram. For the numerical computation of a bifurcation diagram, the rotor speed was increased (decreased) in a constant step and the state variables at the end of an integration were used as the initial values for the next speed. This means that there was a tendency for the integration to follow a single response curve. The Y-coordinate of the return point in the Poincaré section was then plotted versus the rotor speed.

Power Spectrum. Two power spectra were computed. First, the power spectrum of the Y-coordinate was computed and it is referred to as the displacement power spectrum. Secondly, 2048 Y-values of the return points were taken and then the corresponding spectrum was computed. This spectrum is referred to as the power spectrum of the Poincaré map.

To avoid aliasing in the displacement power spectrum, a "long" spectrum was produced by using a small sampling interval and, then, only the first part of the whole spectrum was plotted. For an aperiodic motion, a Hanning window was used to reduce leakage effect. For a subharmonic motion of nth order, the number of driving cycles was taken to be a multiple of n and a rectangular window was used. The frequency axis of the power spectrum plot was normalized using the rotor speed.

5 Results and Discussions

CASE 1: $\epsilon_0 = 0.3$

Approximate Solution and Its Stability. For $U = 0.3$, $B = 0.072$ and $(X_0, Y_0) = (0.0, -0.3)$, the rotor unbalance response was first approximated by an offset ellipse of $\{h\} = \{1\}$ with $N = 1$. It was found that the solution did not converge at speeds around the resonance and so higher-order approximations were required. After some initial trial computations, it was found that a T-periodic solution of $\{h\} = \{1.0, 2.0, 3.0, 4.0\}^T$ with $N = 4$ was satisfactory both in terms of the error criteria and computation time and the coefficients of any higher harmonics remain small.

The second, third, and fourth harmonic terms only become significant at speeds close to the resonance. A T-periodic solution is taken to mean that the least common period of the solution is the period of the driving force. Some components of the predicted unbalance response are given Fig. 3, from which one can note that multiple solutions were predicted

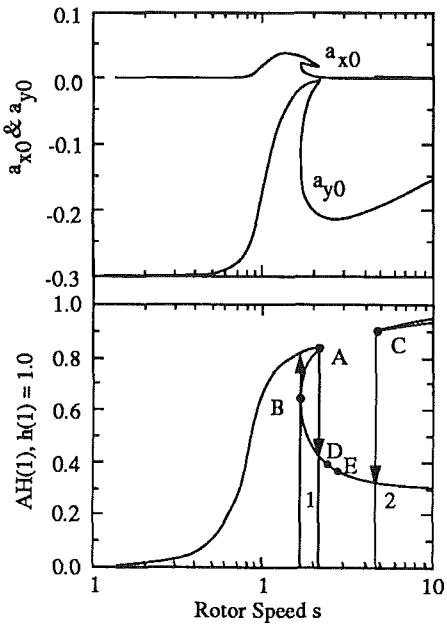

Fig. 3 Unbalance response of T-periodic solution (Case 1)

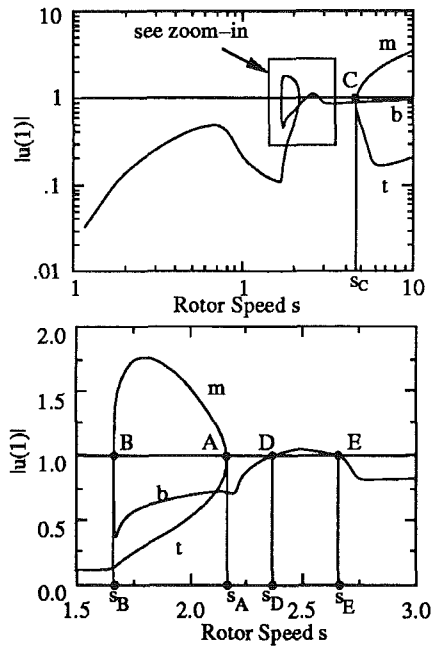

Fig. 4 Absolute value of the leading multiplier of the periodic solution given in Fig. 3

within two speed regions, namely, the first and second multiple-solution regions. It is noted that multiple solutions occur in both the static and harmonic components of the solution. This means that the jump phenomena is characterized by changes in both the amplitude and location of the orbit.

Figure 4 shows the variation of the absolute value of the corresponding leading multiplier with rotor speed. The symbols m, b, and t denote the multipliers corresponding to the middle, lower, and upper branches, respectively. Examining Fig. 4, it is noted that in the two multiple-solution regions the solutions on the upper and lower branches are stable and the solutions on the middle branches are unstable.

The imaginary part of the leading multiplier versus the real part is shown in Fig. 5, from which it can be noted that the transition between the stable solutions and the unstable solutions is characterized by this multiplier crossing the unit circle

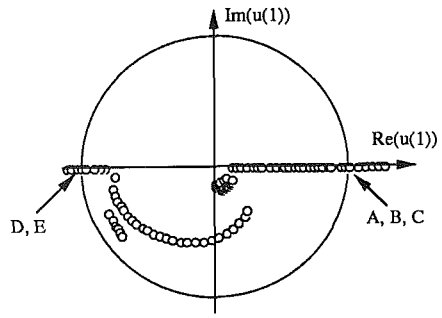

Fig. 5 Imaginary part of the leading multiplier versus real part

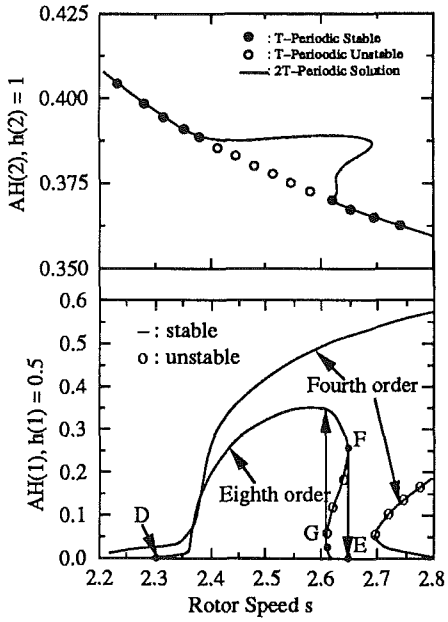

Fig. 6 Semi-major axes of harmonic and subharmonic components of $2T$-periodic solution

at (1, 0). Therefore, any disturbance to an unstable solution will cause the rotor to jump to a stable limit cycle, i.e., to either of the two stable solutions of the same type for this set of parameters. This instability shows the usual jump and the hysteresis loop in the response curve. The stability at the three critical points depends on the nonlinear terms, which have been omitted in the previous linear stability analysis.

The solutions on the single branch are stable except for those on branch DE ($s_D = 2.3$, $s_E = 2.655$). Examination of Fig. 5 indicates that the instability of the solutions on branch DE is characterized by the leading multiplier crossing the unit circle at $(-1, 0)$. This suggests that there is a possibility of buildup of the 0.5-subharmonic motion, that is, a bifurcation from the T-periodic motion to a $2T$-periodic motion on passing point D during run up and passing point E during run down.

To search for such a $2T$-periodic solution, a fourth-order $2T$-periodic approximation of $\{h\} = \{0.5, 1, 1.5, 2\}^T$ was used initially, and the semi-major axes of the subharmonic component of the solution is shown in Fig. 6. However, in this speed region, the nonlinear iteration showed poor convergence in terms of the error criteria, defined as the norm of the residual of the nonlinear algebraic equations, obtained after substituting the approximate solution into differential equations at selected collocation points.

To include both the subharmonic and the fourth superharmonic, an eighth-order approximation of $\{h\} = \{0.5, 1, 1.5, 2, 2.5, 3, 3.5, 4\}^T$ was used. The results also are shown in Fig. 6, together with the synchronous component of the T-periodic

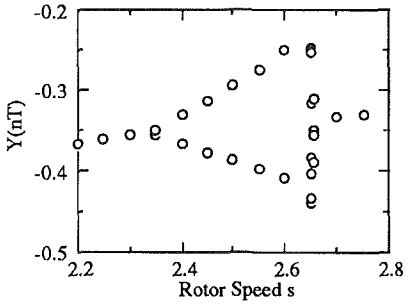

Fig. 7 Bifurcation diagram $Y(nT)$ versus rotor speed

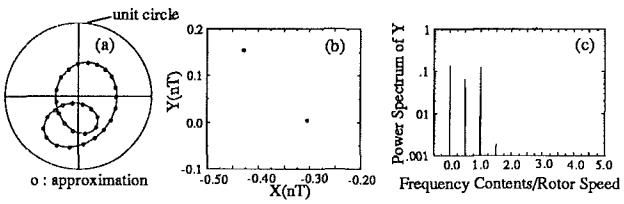

Fig. 8 Subharmonic motion at $s = 2.5$; (*a*) Rotor trajectory; (*b*) Poincaré map; (*c*) Displacement power spectrum

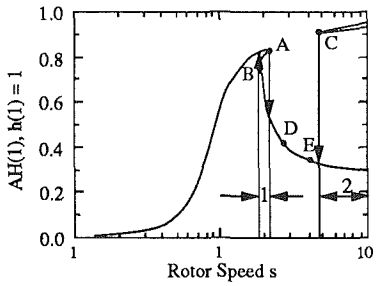

Fig. 9 Semi-major axis of the first harmonic of T-periodic solution versus rotor speed (Case 2)

solution. Again, coefficients for harmonics greater than the fourth remained small. From Fig. 6, it can be seen that on passing point D during run up, the 0.5-subharmonic motion continuously builds up but vanishes suddenly at point F. During run down, the 0.5-subharmonic motion slowly builds up and then suddenly jumps to a large amplitude at the tangent of the curve (point G). There are three solutions in the region of G–F. Stability analysis indicates that the solutions on the upper and lower branches are stable and the solutions on the middle branch are unstable. The transition between the stable and unstable solutions also is characterized by the leading multiplier crossing the unit circle at (1, 0).

Results of Numerical Integration. Figure 7 shows the bifurcation diagram for $2.2 < s < 2.8$. As the speed is increased, the T-periodic motion loses its stability at $s = 2.36$ and a $2T$-periodic motion starts to build up. As the speed is further increased, the $2T$-periodic motion loses its stability at $s = 2.65$ and a T-periodic motion suddenly appears.

The rotor trajectory (shown as a solid line), the Poincaré map, and the displacement power spectrum at $s = 2.5$ are given in Fig. 8, from which the 0.5-subharmonic motion is shown by the double loops of the rotor trajectory, two discrete points in the Poincaré map and peaks at 0.5 in the power spectrum. For comparison, the trajectory predicted by the eighth-order approximation is shown as circles and it can be seen that it lies on the numerically integrated trajectory.

Thus, it can be seen that the eighth-order approximation was necessary to describe the response in the region of the subharmonic resonance for larger static misalignments, but little improvement was gained by using the eighth-order over the fourth-order approximation for small misalignments.

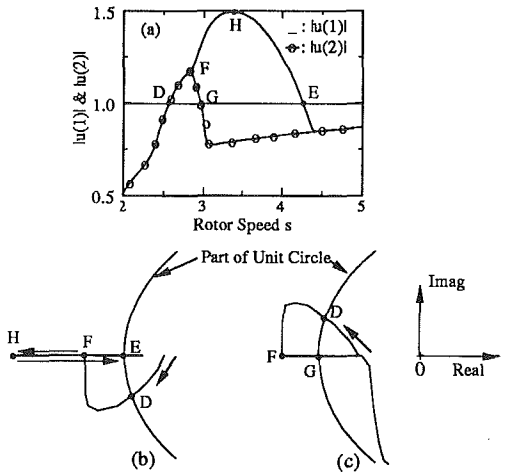

Fig. 10 First two Floquet Multipliers of the T-periodic solution shown in Fig. 9 versus rotor speed. (*a*) Absolute values of $u(1)$ and $u(2)$; (*b*) Imaginary of $u(1)$ versus real; (*b*) Imaginary of $u(2)$ versus real.

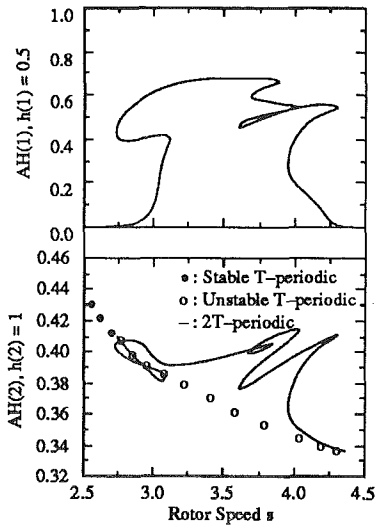

Fig. 11 Semi-major axes of the subharmonic and harmonic components of $2T$-periodic solution versus rotor speed

CASE 2: $\epsilon_0 = 0.7$

Approximate Solution and Its Stability. Figure 9 is the approximate T-periodic solution for an increased static misalignment of $\epsilon_0 = 0.7$ ($X_0 = 0.0$, $Y_0 = -0.7$). The rest of parameters remained unchanged. For this set of parameters, multiple solutions were again predicted over two speed regions.

Examination of the corresponding multipliers indicates that the local stability of the multiple solutions are similar to that of Case 1, i.e., the solutions on the upper and lower branches are stable, while the solutions on the middle branch are unstable. The transition between the stable solutions and the unstable solutions also is characterized by the leading multiplier crossing the unit circle at (1, 0).

It also may be seen that the solutions on the single branch are stable except for those on branch DE, for which the stability is determined by the first two multipliers, as shown in Fig. 10. From this figure, it can be noted that a pair of complex-conjugate multipliers cross the unit circle at $s_D = 2.56$ and thus the T-periodic motion becomes unstable at this speed. Crossing the unit circle with a pair of complex-conjugate multipliers indicates a bifurcation from the T-periodic motion into a two-dimensional torus having two irrational fundamental frequencies ω_1 and ω (ω is the rotor speed). At point F ($s_F = 2.89$), the imaginary parts of the pair of complex-conjugate multipliers

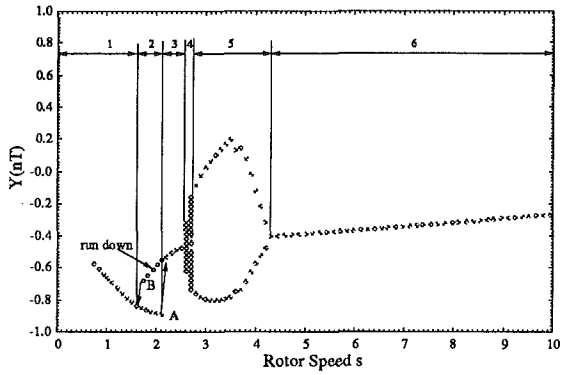

Fig. 12 Local bifurcation diagram $Y(nT)$ versus rotor speed s (case 2)

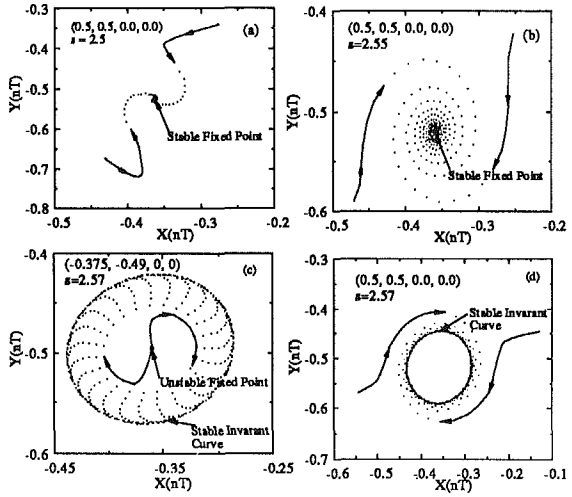

Fig. 13 Transient behavior of Poincaré section near the secondary Hopf bifurcation point

become zero and the corresponding two real multipliers move in the opposite direction along the real axis as the speed is further increased. This indicates a locking to a 0.5-subharmonic motion. On passing point G ($s_G = 2.95$), the second multiplier moves inside the unit circle and the stability of the approximate solutions beyond this speed is governed by the first multiplier alone. On passing point E ($s_E = 4.25$), the first multiplier also moves inside the unit circle and the 0.5-subharmonic motion bifurcates into a T-periodic motion.

To seek a 2T-periodic solution between s_D and s_E, an eighth-order 2T-periodic approximation of $\{h\} = \{0.5, 1.0, 1.5, 2.0, 2.5, 3.0, 3.5, 4.0\}^T$ was used and the results are given in Fig. 11, together with the synchronous component of the T-periodic solution. The loopbacks, shown in Fig. 11, do not appear to have a satisfactory physical interpretation and raise the question of the necessity for higher-order approximations, which would, in turn, involve prohibitively large amounts of computational time. Therefore, numerical integration was used to establish the accuracy of the series solution as follows.

Results of Numerical Integration

Figure 12 shows the bifurcation diagram obtained by integrating the differential equations with nonzero initial values starting from $s = 0.0$ for 800 driving cycles at each of the rotor speeds. The first 500 cycles were discarded to insure that only the steady-state behavior was plotted. This bifurcation diagram shows regions of periodic and aperiodic motions, which was considered in terms of six speed ranges.

$0 < s < 1.59$ (Region 1). In this region, the rotor motion is T-periodic as predicted approximately.

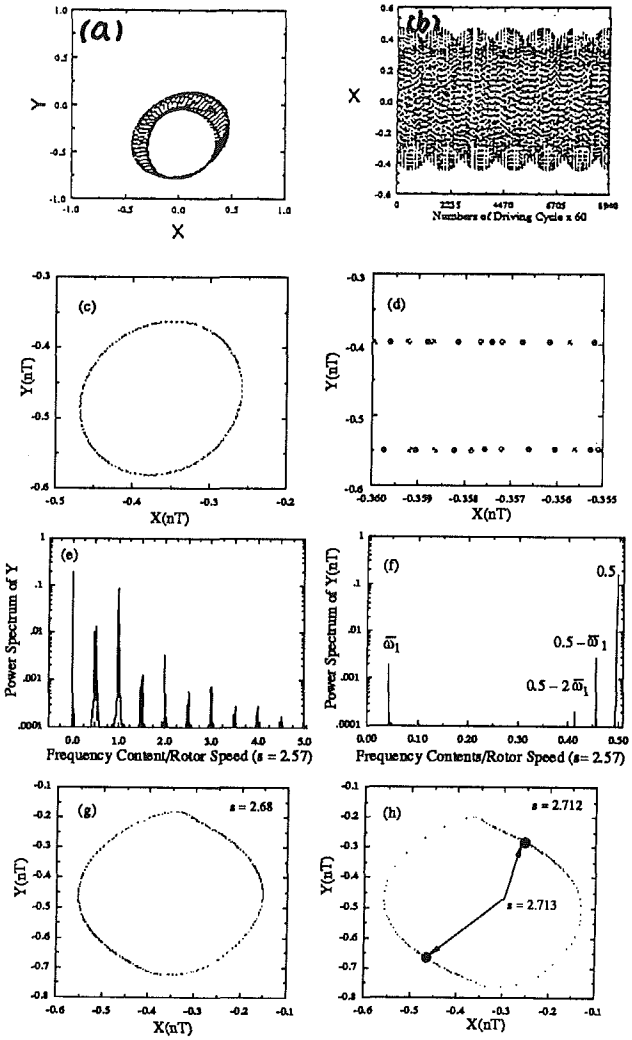

Fig. 14 Quasi-periodic motion in Region 4 of Fig. 12 (a–f) $s = 2.57$. (a) Rotor trajectory; (b) Displacement; (c) Poincaré map; (d) Zoom-in of (c); (e) Displacement power spectrum; (f) Spectrum of Poincaré map; (g–h) Poincaré maps at $s = 2.68$, 2.712, and 2.713.

$1.59 < s < 2.17$ (Region 2). Here, there are two stable T-periodic motions—which of them the rotor actually follows depends on the initial condition. During run up, a T-periodic motion jumps to another T-periodic motion at $s = 2.17$ (point A) and a reverse jump occurs at $s = 1.59$ (point B) during run down. The unstable middle branch predicted, using the approximate solution, was unable to be confirmed using the integration method.

$2.17 < s < 2.56$ (Region 3). In this region, there is a T-periodic motion as predicted approximately.

$2.56 < s < 2.712$ (Region 4). Here the rotor motion is aperiodic. At $s = 2.56$, the T-periodic motion bifurcates into a quasi-periodic motion. Figure 13 shows the transient behavior of the Poincaré maps near $s = 2.56$. The initial values, $(X, Y, \dot{X}, \dot{Y})$, for the numerical integration also are given in the figure. At $s = 2.5$ in Fig. 13(a), the convergence of return points shows a spiralling characteristic. At $s = 2.55$ in Fig. 13(b), the rate of convergence is remarkably slower and, at $s = 2.57$ in Fig. 13(c), return points move outward toward the stable, invariant curve from near the unstable fixed point. Figure 13(d) shows the approach to the stable invariant curve from the outside.

Figure 14 shows a typical quasi-periodic motion at $s = 2.57$. The rotor trajectory and the time series for 150 driving cycles, after the first 2000 transient cycles, are given in Figs. 14(a)

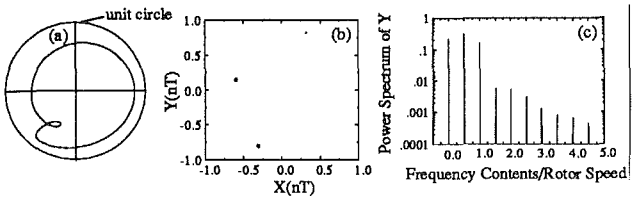

Fig. 15 Subharmonic motion at $s = 3.5$. (*a*) Rotor trajectory; (*b*) Poincaré map; (*c*) Displacement power spectrum.

and (b), from which it can be seen that the trajectory fills up a bounded space. The time series shows an amplitude modulated motion with the second fundamental frequency being about 1/25 of the rotor speed. The Poincaré map and its zoom-in are shown in Figs. 14(c) and (d), respectively, and it may be seen that return points wind round and fill up a closed curve (a drift ring), but never coincide precisely with any previous return point. The displacement power spectrum in Fig. 14(e) shows that the 0.5-order subharmonic motion is modulated by a frequency component of $\omega_1 \cong 0.04\omega$ and, therefore, it has peaks at the combination frequencies of $m/2 \pm \omega_1$, m, $n = 0$, ± 1, ± 2 . . . . The normalized second fundamental frequency $\bar{\omega}_1$ is clearly shown in the power spectrum of the Poincaré map in Fig. 14(f).

For comparison, the Poincaré maps for three increased speeds are given in Figs. 14(g) and (h), from which it can be seen that as the speed is increased, return points advance rapidly in the regions where points are visibly scarce and advance slowly in two regions where points are visibly dense. At $s = 2.713$ in Fig. 14(h), the quasi-periodic motion locks into a $2T$-periodic motion in a catastrophic way.

$2.712 < s < 4.25$ (Region 5). Here the rotor motion is $2T$-periodic. The $2T$-periodic rotor motion at $s = 3.5$ is given in Fig. 15, from which it can be noted that the rotor trajectory exhibits double loops and the Poincaré map consists of two discrete points. The displacement power spectrum has peaks at frequencies of $m\omega/2$. As the speed is further increased, the two discrete points in the Poincaré map move closer and coincide to a fixed point at $s = 4.25$. This indicates that the $2T$-periodic motion bifurcates into a T-periodic motion in a subtle way.

$4.25 < s < 10$ (Region 6). Here there is a T-periodic motion. For $s > 4.5$, the numerical integration failed to find the approximately predicted stable and unstable rotor motions having large amplitudes for the initial values used.

6 Conclusions

The stability and bifurcation of the approximate analytical unbalance response of an eccentric squeeze-film damper-supported rigid rotor has been determined. By examining the way in which an approximate analytical solution becomes unstable, the motion in the neighborhood of the unstable solution was able to be estimated. For large values of the unbalance and the static misalignment, it was shown that the subharmonic and quasi-periodic motions at above twice the system critical speed were bifurcated from the unstable harmonic solution. The approximate analytical bifurcation values of the rotor speed are very close to those obtained by the numerical integration. The substantial differences between the lower and higher-order approximations necessitates the inclusion of higher-order terms for larger values of the static misalignment.

The results of this study provide a further understanding of the nonlinear dynamics of rotor damper systems and it was shown that the introduction of dampers may give rise to the undesirable nonsynchronous vibrations, which may limit the maximum speed at which dampers should be used.

References

Arnol'd, V. I., 1983, *Geometrical Methods in the Theory of Ordinary Differential Equations*, New York, Springer-Verlag.

Botman, M., 1976, "Experiments on Oil Film Dampers for Turbomachinery," TRANS. ASME *Journal of Engineering for Power*, Vol. 98, pp. 393–400.

Feng, N. S., 1988, "Cavitation Effects on Squeeze Film Damper Performance," PhD Thesis, The University of New South Wales, Australia.

Li, X. H., and Taylor, D. L., 1987, "Nonsynchronous Motion of Squeeze-Film Damper Systems," TRANS. ASME *Journal of Tribology*, Vol. 109, Jan., pp. 169–176.

Mohan, S., and Hahn, E. J., 1974, "Design of Squeeze-Film Damper Supports for Rigid Rotors," TRANS. ASME *Journal of Engineering for Industry*, Aug., pp. 976–982.

Nataraj, C., and Nelson, H. D., 1989, "Periodic Solutions in Rotor Dynamic Systems with Nonlinear Supports: A General Approach," TRANS. ASME *Journal of Vibration, Acoustics, Stress, and Reliability in Design*, Vol. 111, pp. 187–193.

Nikolajsent, J. L., and Holmes, R., 1979, "Investigation of Squeeze-Film Isolators for the Vibration Control of a Flexible Rotor," TRANS. ASME *Journal of Mechanical Science*, Vol. 21, No. 4, pp. 247–252.

Sykes, J. E. H., and Holmes, R., 1990, "The Effects of Bearing Misalignment on the Nonlinear Vibration of Aero-Engine Rotor-Damper Assemblies," *Proceedings of the Institute of Mechanical Engineers*, Part G, *Journal of Aerospace Engineering*, Vol. 24, pp. 83–99.

White, D. C., 1970, "Squeeze-Film Journal Bearings," PhD thesis, Churchill College, The University of Cambridge.

Zhao, J. Y., Linnett, I. W., and McLean, L. J., 1993, "Unbalance Response and Stability of Eccentric Squeeze Film Damped Nonlinear Rotor Bearing Systems," to be published by JSME, Paper No. 93-3021.